CAN FRACTALS MITIGATE BLAST LOADING?

Sam RIGBY[1], Obed ISAAC[2], Omar ALSHAMMARI[3] & Sam CLARKE[4]

Abstract: *Fractals are self-similar objects; a shape or pattern made up of an infinitely repeating series of smaller copies of the original. Self-similarity is common in nature – trees, coastlines, shells – and infinitely-repeating fractals possess the interesting characteristic of having finite volume but* infinite *surface area (hence the 'Coastline Paradox'). Whilst it is not possible to achieve infinite fractal iterations in real-life, pre-fractals (a self-similar structure with a* finite *number of iterations) have a sufficiently large area:volume ratio to be useful in a number of engineering applications, such as antennae and heat exchangers. The properties of a blast wave are substantially altered after it comes into contact with an obstacle: reflection of the wavefront diverts the blast away from its primary path, and diffraction around the obstacle edge induces vortices and further diverts momentum. This raises an interesting question:* can fractals mitigate blast loading*? Specifically, does the large area:volume property of pre-fractal obstacles increase the propensity for a blast wave to divert energy away from its original path, thereby mitigating the blast load downstream of the obstacle? This paper details a rigorous experimental study on the blast mitigation of the first three iterations of a* Sierpinski carpet *subjected to the blast load from PE4 explosives, with downstream, upstream, and on-obstacle pressures directly measured by flush-mounted pressure gauges. The results show that mitigation is enhanced with increasing iteration number, and that the mitigation behaviour of a pre-fractal obstacle is fundamentally different to that of a simple, singular obstacle. This proof-of-concept study opens up the possibility of using natural self-similar structures, such as trees and hedges, for sustainable and less intrusive blast protection in urban environments.*

Introduction

Background

In order to protect civilians and infrastructure against the damaging effects of explosions, a crucial first step is to understand and quantify the magnitude and form of blast loading generated in these situations. Recent events such as the 2020 Beirut explosion (Rigby et al. 2020) and the current conflict in Ukraine have highlighted the need to better understand explosions in complex environments. That is, whist the propagation of a blast wave in a free-air (unobstructed) environment may be well understood and readily predicted by simple tools, coalescence of multiple shock fronts that have reflected off or diffracted around obstacles is a highly non-linear physical process and simple predictive approaches are no longer valid (Larcher and Casadeia 2010). Clearly, the provision of efficient and effective protective systems is not possible without a firm understanding of the interaction of blast waves with obstacles.

Blast protection in its simplest form can be achieved through the use of purpose-built hardened structures which serve to shield the target from the damaging aspects of blast and fragmentation, whilst diverting the blast back towards the source and potentially absorbing energy through mechanical work (Smith 2010). Clearly, the primary requirements here are a massive, robust structure with little consideration of sustainability aspects (including material use and perception of risk/danger amongst the general public).

Alternatively, blast pressure can be mitigated through blast-obstacle interaction, e.g. allowing the blast to propagate through – and interact with – a porous obstacle and/or an array of smaller structures, such as forests, trees, and hedges (Suzuki et al. 2000, Gebbeken, Warnstedt and Rüdiger 2018, Gan, Remennikov and Ritzel 2021, Gajewski et al. 2022). Here, the properties of a blast wave can be substantially reduced due to the dual aspects of diversion of the wavefront away from its primary path, and diffraction around the obstacle edge(s) inducing vortices and

---

[1] Senior Lecturer in Blast & Impact Engineering, University of Sheffield, Sheffield, UK, sam.rigby@shef.ac.uk
[2] Research Associate in Blast Propagation Mechanics, University of Sheffield, Sheffield, UK
[3] PhD Student, University of Sheffield, Sheffield, UK
[4] Professor of Blast Geotechnics, University of Sheffield, Sheffield, UK

further diverting momentum. Utilising porous structures in urban blast protection settings is likely to be significantly less obtrusive than traditional monolithic blast walls. The aim of this study is to investigate the blast mitigation behaviour of such an array of smaller structures, with the overall goal of better understanding these new, sustainable, nature-inspired blast protection systems.

Fractals in engineering

Trees and hedges are an example of naturally occurring fractal-like structures. Fractals are self-similar objects; a shape or pattern made up of an infinitely repeating series of smaller copies of the original. Self-similarity is common in nature – trees, coastlines, shells – and infinitely-repeating fractals possess the interesting characteristic of having finite volume but *infinite* surface area, as exemplified by the 'Coastline Paradox' (https://en.wikipedia.org/wiki/Coastline_paradox) where the length of a coastline appears to increase with increasing measurement resolution. A true fractal is a mathematical idealisation; an *infinite* number of iterations of a particular shape or pattern. Hence, the term 'pre-fractal' is used to describe a self-similar structure with a *finite* number of iterations.

Pre-fractal obstacles have an increasing area:volume ratio with increasing iteration number. This makes high-iteration pre-fractal obstacles particularly suited to a number of engineering applications such as antennae, industrial mixing, and heat exchangers. High iteration pre-fractal structures also exhibit enhanced crashworthiness (Nguyen et al. 2021) and increased downstream turbulence and vorticity in flow problems (Higham and Vaidheeswaran 2022). Additionally, the presence of multiple length scales substantially increases edge effects (e.g. diffraction and vortex shedding) for a given volume of obstacle. This leads to the main scientific question of this study: *can fractals mitigate blast loading?* Specifically, does the large area:volume property of pre-fractal obstacles increase the propensity for a blast wave to divert energy away from its original path, thereby mitigating the blast load downstream of the obstacle? This is addressed through a comprehensive experimental study, as is detailed in the following sections.

Experimental design

The Sierpinski carpet is a common fractal shape formed by dividing a square domain into a 3×3 grid, removing the central sub-square, and recursively iterating the process for the remaining sub-squares. This concept is adapted for this study, however the centre of each square/sub-square is *filled* (i.e. the domain begins as empty, rather than full). Preliminary numerical modelling studies indicated that, given a charge mass of 250 g, a central obstacle width of 180 mm would result in noticeable mitigation behaviour (Alshammari et al. 2022) with obstacle sizes that could be readily fabricated and installed on site. Accordingly, the following arrangements were tested:

- *"iteration 0"*: free-field incident trials with no obstacle present
- *"iteration 1"*: inclusion of a central, 1 m high, 180 mm square obstacle
- *"iteration 2"*: as above, with inclusion of eight 1 m high, 60 mm square obstacles surrounding the central obstacle (with a 60 mm gap)
- *"iteration 3"*: as above, with inclusion of eight 1 m high, 20 mm square obstacles surrounding each of the eight 60 mm square obstacles (with a 20 mm gap).

The first three iterations of a Sierpinski carpet are shown schematically in Figure 1, and images of the as-built pre-fractal obstacles are shown in Figure 2. The obstacles were fabricated from square steel sections, or solid steel rods for the 20 mm obstacles, and the area:volume ratios of each iteration are 0.222, 0.431, and 0.894 respectively. Full details of how the pre-fractal obstacles were manufactured and installed are available in Isaac et al. (2022a).
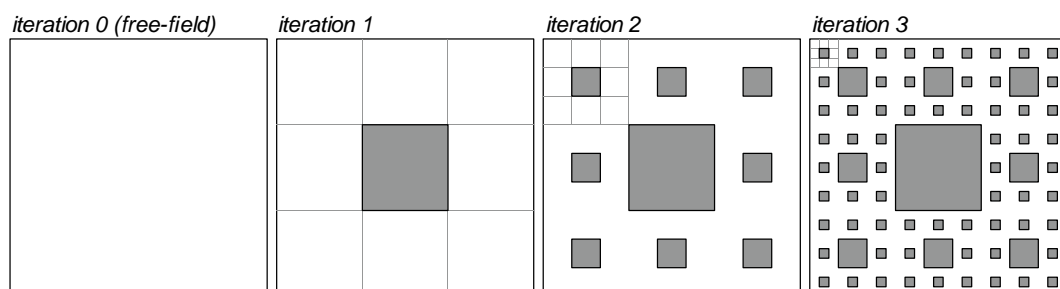

Figure 1. Schematic of the first three iterations of a Sierpinski carpet (plan).

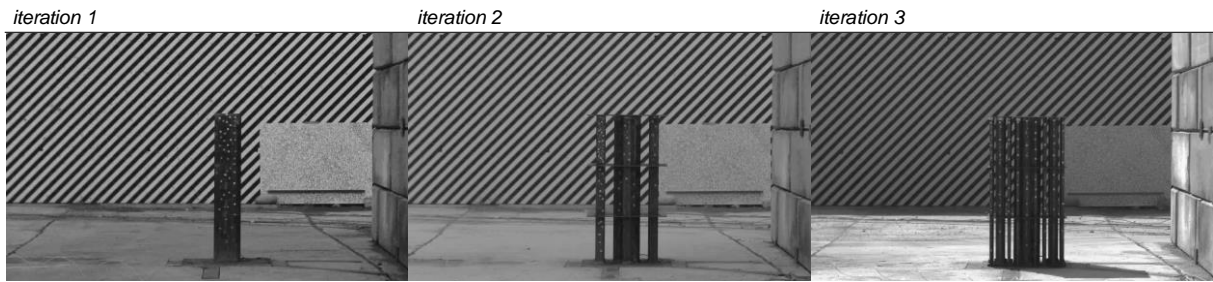*iteration 1*   *iteration 2*   *iteration 3*

Figure 2. High speed video stills showing the as-constructed obstacles for each iteration (elevation).

Experimental set up

A total of 45 tests were performed at the University of Sheffield Blast & Impact Laboratory, Buxton, UK, of which 38 were instrumented trials and seven were commissioning tests. 250 g hemispherical PE4 charges were used throughout and were centrally-detonated at stand-off distances between 1.25 and 2.00 m from the front-face of the central obstacle. Experimental results are reported in full in Isaac et al. (2022a). Free-field (iteration 0) test data from all stand-off distances is briefly reported in the subsequent section, otherwise iteration 1–3 data presented in this article are from the 1.25 m stand-off tests only, comprising 12 tests in this subset.

Whilst the physical processes governing blast attenuation through blast-obstacle interaction are known to be a function of shock strength (Isaac et al. 2022b, Alshammari et al. 2022), and, implicitly, stand-off distance, findings from the 1.25 m tests are generally representative of the entire test series since the form of the obstacle (i.e., pre-fractal iteration) has a primary influence on blast-obstacle interaction, and shock strength has a secondary influence.

The test arena was instrumented with 12 piezo-resistive dynamic pressure sensors (see Figure 3), in one of five categories:

- "*upstream*": S10 and S11, those between the obstacle and the explosive
- "*lateral*": S8 and S9, those adjacent to the obstacle
- "*downstream*": S4–7, those behind the obstacle
- "*on-target*": S12, on the front-face of the central obstacle
- "*reflected*": S1–3, those embedded in a nominally rigid blockwork wall behind the obstacle.
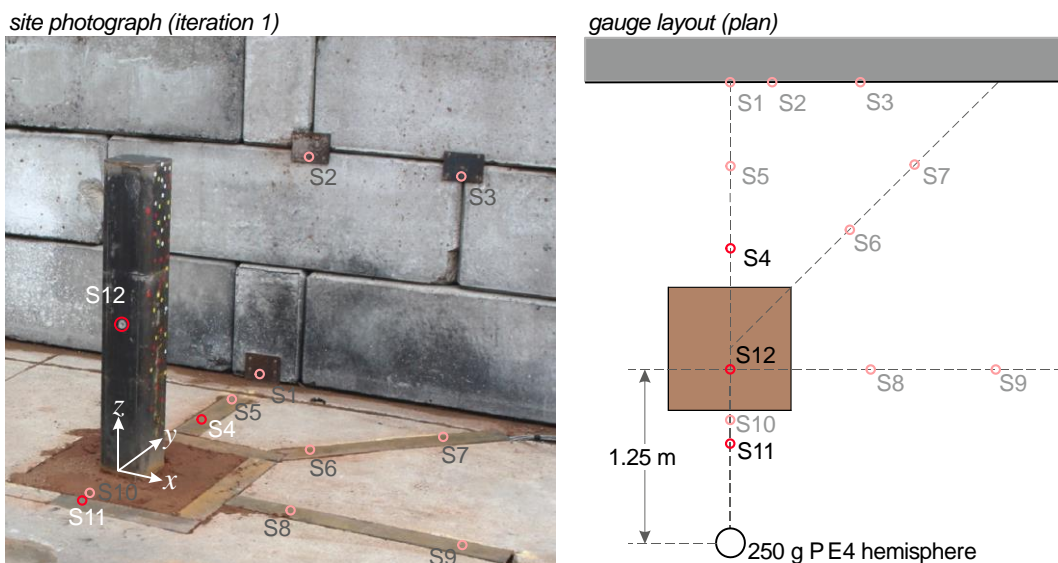

Figure 3. Site photograph and plan view of the sensor locations.

Pressure data were recorded at a sampling frequency of 312.5 kHz, and recordings were synchronized with detonation using a break-wire wrapped around the detonator. S1–3 were mounted in small steel plates which were affixed to the surface of the blockwork wall, and S4–11 were mounted in steel C-sections which were sat in small channels that had been cut into the

concrete test pad which were then backfilled with sand and levelled off to ensure a smooth ground surface. S12 was secured in a small metal bush that was mounted in the front face of the central obstacle. Note: this sensor was not used in the iteration 0 free-field trials due to the absence of the central obstacle. In all cases, pressure sensors were mounted flush with the surface in which they were embedded in (ground, blockwork wall, and central obstacle).

Only results from S4, S11 and S12 are presented in full this article (again, test data from *all* sensor locations are only reported for the iteration 0 tests), with coordinates of the relevant locations provided in Table 1. Note that [0, 0, 0] corresponds to the bottom-centre of the front-face of the central obstacle, as indicated in Figure 3.

Object	[	$x,$	$y,$	z]	Terminology
Explosive	[	0,	-1.25,	0]	
Sensor 4	[	0,	0.55,	0]	*"Downstream"*
Sensor 11	[	0,	-0.30,	0]	*"Upstream"*
Sensor 12	[	0,	0,	0.51]	*"On-obstacle"*

Table 1. Coordinates of explosive charge and pressure sensors reported in this article.

Results

Iteration 0 (free-field)

Before studying the effects of blast-obstacle interaction in the iteration 1–3 tests, it is important to first assess the repeatability and reliability of the iteration 0 tests, such that any trends in the obstructed test can be attributed to genuine behaviour rather than experimental spread or some underlying uncertainty. Figure 4 shows peak pressure and peak specific impulse from all incident sensors (S4–11) for all tests. Here, peak pressure is taken as the maximum recorded pressure after the traces had been de-noised with a 5th order wavelet filter (Isaac et al. 2022a), and peak specific impulse is determined through cumulative numerical (trapezoidal) integration. The results are compared against UFC predictions (US DoD 2008) assuming a TNT equivalence of 1.20 for PE4 (Rigby and Sielicki 2014).
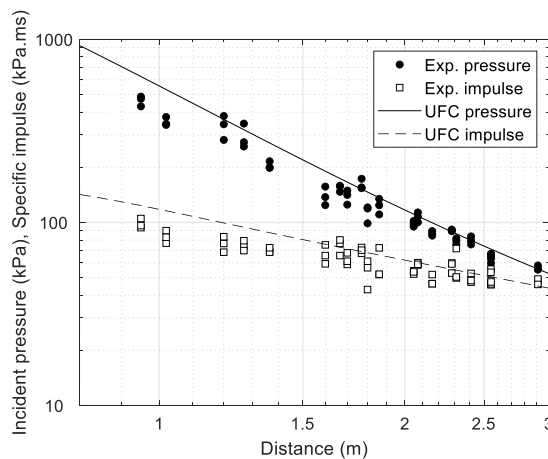

Figure 4. Compiled peak pressure and specific impulse for all incident sensors.

Generally the results are in good agreement with the UFC predictions, with agreement seen to improve with increasing distance from the charge: deviations of >30% are seen at the closest distances, whereas deviations of <5% are typical at the furthest distances (for both pressure and impulse). Rather than being suggestive of some deterioration in the quality of experimental data at shorter stand-off distances, it is suggested that this is in fact due to some systemic conservatism in the UFC predictions, as has been reported in other sources e.g., Bogosian, Ferrito and Shi (2002). Therefore, suitable reliability and consistency of the free-field test data has been established.

Iterations 1–3; "Downstream" pressure

Figure 5 shows pressure and specific impulse histories recorded at S4 for the 1.25 m stand-off tests (i.e., 1.25 m from the explosive to the obstacle, 1.80 m distance from the explosive to the

sensor), with increasing iterations of the Sierpinski carpet pre-fractal. Results from iteration 0 (averaged in time for the three repeat tests) are shown in red for comparison.

It can be seen that immediately downstream of the iteration 1 obstacle (comprising the 180 mm square central obstacle only) there is a slight increase in both peak pressure and specific impulse, likely due to the wavefront separating, diffracting around the obstacle, and reforming/coalescing before reaching the sensor location. There is a slight increase in arrival time, and the pressure history is similar in form to the equivalent free-field trace.

For iteration 2, peak pressure is again slightly increased, albeit less so than for iteration 1, and peak specific impulse is similar to the free-field value. Arrival time is more substantially increased and the waveform differs significantly from the iteration 1 case, which is indicative of a more disrupted reforming of the wavefront. For iteration 3, arrival time is significantly increased and peak pressure and specific impulse are considerably lower than the free-field values. The waveform is altogether much more complex than the free-field trace, suggesting that a more complete separation of the wavefront is achieved, and that it gradually reforms over time, resulting in considerable attenuation and mitigation of the blast load.
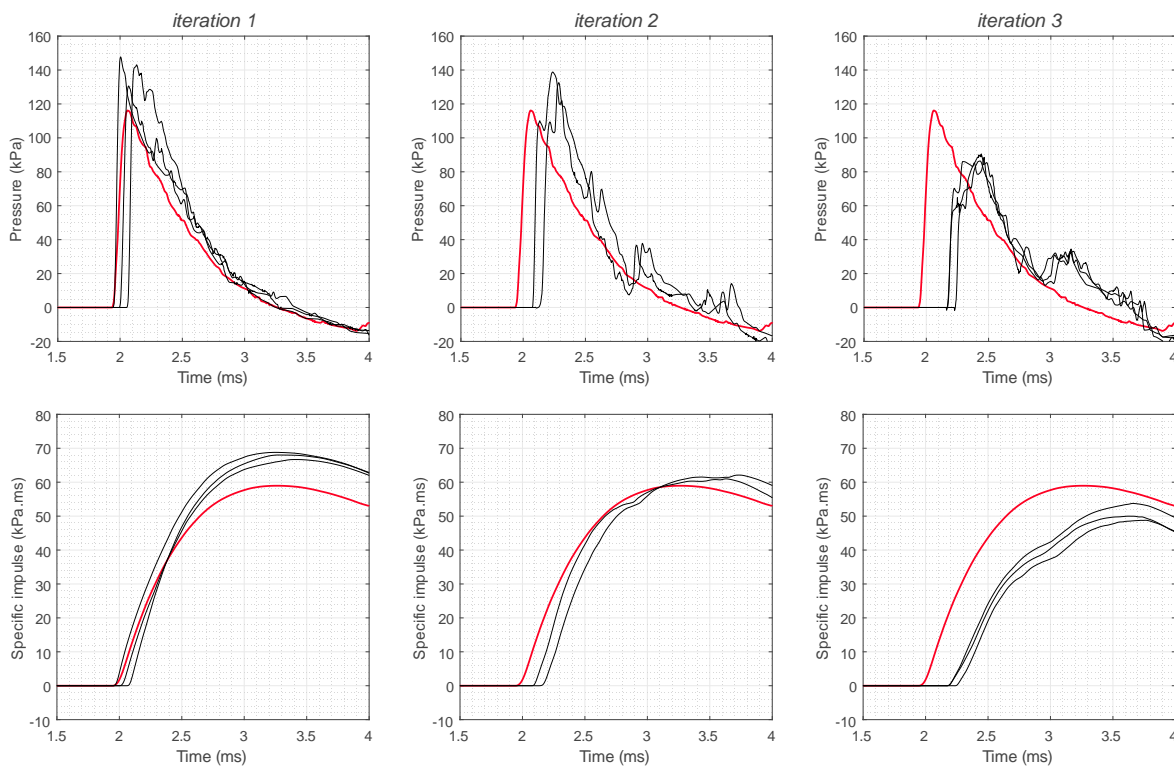

Figure 5. "Downstream" incident pressure and specific impulse histories (S4; 1.80 m from a 250 g PE4 hemisphere). Iteration 0 results shown in red.

Iterations 1–3; "Upstream" pressure

Figure 6 shows pressure and specific impulse histories recorded at S11 for the 1.25 m stand-off tests (i.e., 1.25 m from the explosive to the obstacle, 0.95 m distance from the explosive to the sensor), again with increasing iterations of the Sierpinski carpet pre-fractal. As previously, results from iteration 0 are shown in red.

Iteration 1 peak pressures are comparable to the free-field values, and whilst peak specific impulses exhibit a relatively large degree of spread[5] they are generally also comparable to, or lower than, the free-field values. Again, the iteration 2 pressure histories are largely comparable to the free-field results, albeit with a slightly increased peak pressure. The traces clearly exhibit the arrival of a secondary loading pulse at approximately 1.3 ms after detonation which is not present in either the iteration 0 or iteration 1 traces. This serves to increase the peak specific impulse slightly above the iteration 0 values. Finally, the waveforms for iteration 3 are

---

[5] Likely due to the proximity of the sensor to the explosive; an increase in blast load variability is commonly seen with shorter scaled distances (Farrimond et al 2022)

considerably more complex. Here, the sensor is only 120 mm clear of the front face of the first line of 20 mm obstacles, which means that large magnitude wave reflections are seen to arrive earlier in the loading pulse. Additionally, the late-time loading pulse is of higher magnitude and arrives earlier compared to the iteration 2, which further highlights the complexity of the blast-obstacle interaction process for the iteration 3 tests. Specific impulse is largest at this sensor for the iteration 3 tests on account of these multiple wave reflections and suggests that a larger proportion of the blast wave is directed back towards the source as obstacle complexity and surface area (i.e., iteration number) increases.
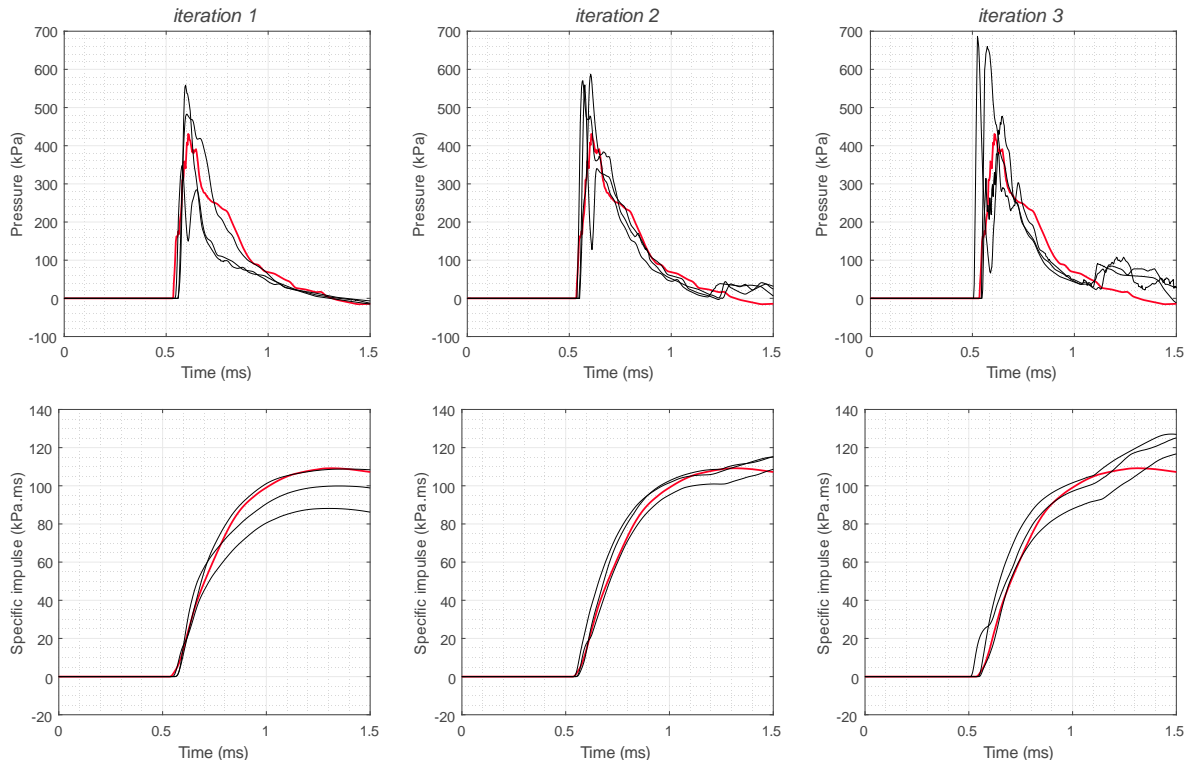

Figure 6. "Upstream" incident pressure and specific impulse histories (S11; 0.95 m from a 250 g PE4 hemisphere). Iteration 0 results shown in red.

Iterations 1–3; "On-obstacle" pressure

Finally, pressure histories on the front-face of the central obstacle are examined in order to investigate how the blast load in the vicinity of the pre-fractal differs with increasing iteration, as in Figure 7. As equivalent free-field test data is not available for this test, UFC (US DoD 2008) incident predictions are shown here for comparative purposes[6].

Considering the iteration 1 pressure history first, the behaviour can be described as follows: initially, the full reflected pressure[7] is developed on the front face of the central obstacle; subsequently, diffraction (clearing) relief waves arrive from the edges of the surface and the pressure pulse quickly reduces to below incident conditions for the remainder of the loading duration. The result is a more rapid accumulation of specific impulse, but the end result is similar to the peak incident specific impulse.

The iteration 2 trace is broadly similar, exhibiting a sharp rise to peak reflected pressure followed by a rapid decay to below ambient conditions, however the arrival of multiple smaller loading peaks (from 1.4 ms onwards) increases the pressure level somewhat, and the signal generally follows the incident trace thereafter. The result is a slightly increased peak specific impulse.

---

[6] Since the central obstacle has a small presented area relative to the blast wavelength, clearing relief is expected to occur completely and therefore the loading magnitudes will more closely resemble the incident pressures, rather than reflected (Rigby et al. 2014)

[7] The pressure will be subjected to progressive clearing seen in Rose, Smith and McLennan (2004) as the blast sweeps up the surface of a 'tall' reflecting surface, hence the peak reflected pressure is significantly lower than the infinite-target UFC prediction (~1 MPa)

The iteration 3 trace is noticeably different from the iteration 1 and 2 traces. The peak reflected pressure is higher in magnitude than the other traces by some 40%, and it remains above the incident conditions throughout, suggesting that clearing around the central obstacle is negated by some other mechanism. A series of additional loading pulses arrive at the sensor location broadly every 0.1 ms, each of which are reflections from the surface of one of the smaller obstacles. This is termed 'trapping' and is a clear indication of a new attenuation mechanism as greater proportion of the wave is diverted from its original. The resulting waveform is highly complex with a peak impulse almost double the incident loading and iteration 1 and 2 traces.
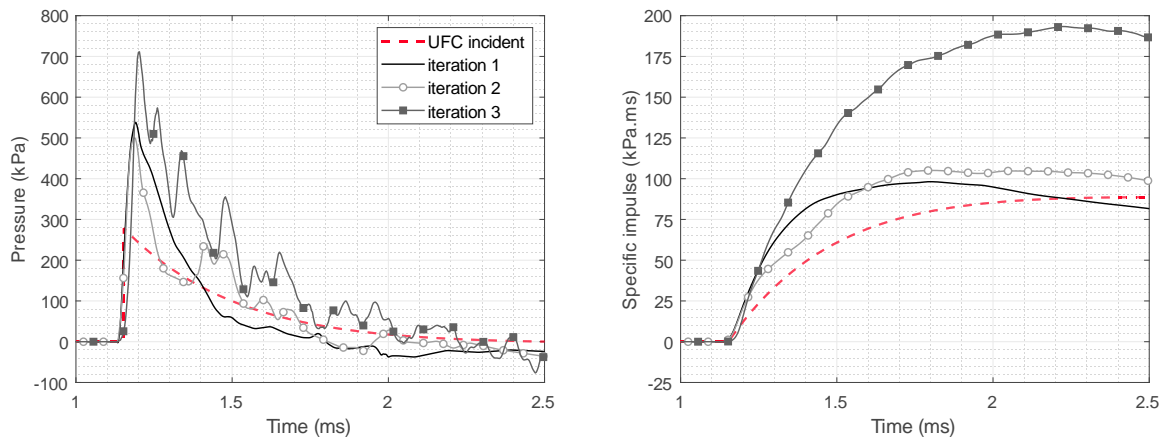

Figure 7. "On-obstacle" reflected pressure and specific impulse histories (S12; 1.35 m slant distance from a 250 g PE4 hemisphere). UFC incident predictions shown in red.

Discussion

Figure 8 shows compiled peak pressure and specific impulse at the three sensor locations, with increasing iteration number. With reference to this figure and the previous pressure traces (Figures 5–7), attenuation appears to be driven by the following mechanisms:

- *"iteration 1"*: the blast wavefront is initially disturbed, but due to the simple nature of the obstacle it quickly coalesces downstream leading to pressure enhancement (S4; ~20% increase). Shielding effects of the obstacle are negated by pressure enhancement as the wave reforms. On-target loading (S12) is relatively simple as drag conditions are quickly established, and the magnitude of the upstream reflected wave is negligible (S11)
- *"iteration 2"*: the blast wavefront is moderately disturbed, and although it reforms downstream this enhancement is counteracted by shielding effects of the obstacle, therefore there is no noticeable downstream attenuation or enhancement (S4). Upstream loading is slightly enhanced (S11; 10-15% increase) due to more substantial wave reflection off the obstacle on account of its greater surface area relative to iteration 1.
- *"iteration 3"*: the blast wavefront is significantly disturbed and no longer coalesces in a single occurrence, therefore downstream attenuation is significant (S4; ~20% reduction). A greater proportion of the wave is reflected back towards the source (S11; ~20% increase) and the on-target loading demonstrates significant trapping effects (S12; ~30% increase in pressure, ~70% increase in impulse). Attenuation is predominantly driven by energy expended during trapping, i.e., through a combination of vortex shedding and the blast being forced along a lengthened travel path.

These findings are significant in that they reveal the presence of a fundamentally different attenuation mechanism for iteration 3 compared to iterations 1 and 2. This suggests that blast mitigation behaviour of trees and hedges is likely due to their fractal-like nature, i.e., self-similarity, presence of multiple length scales, and high surface area to volume ratio.
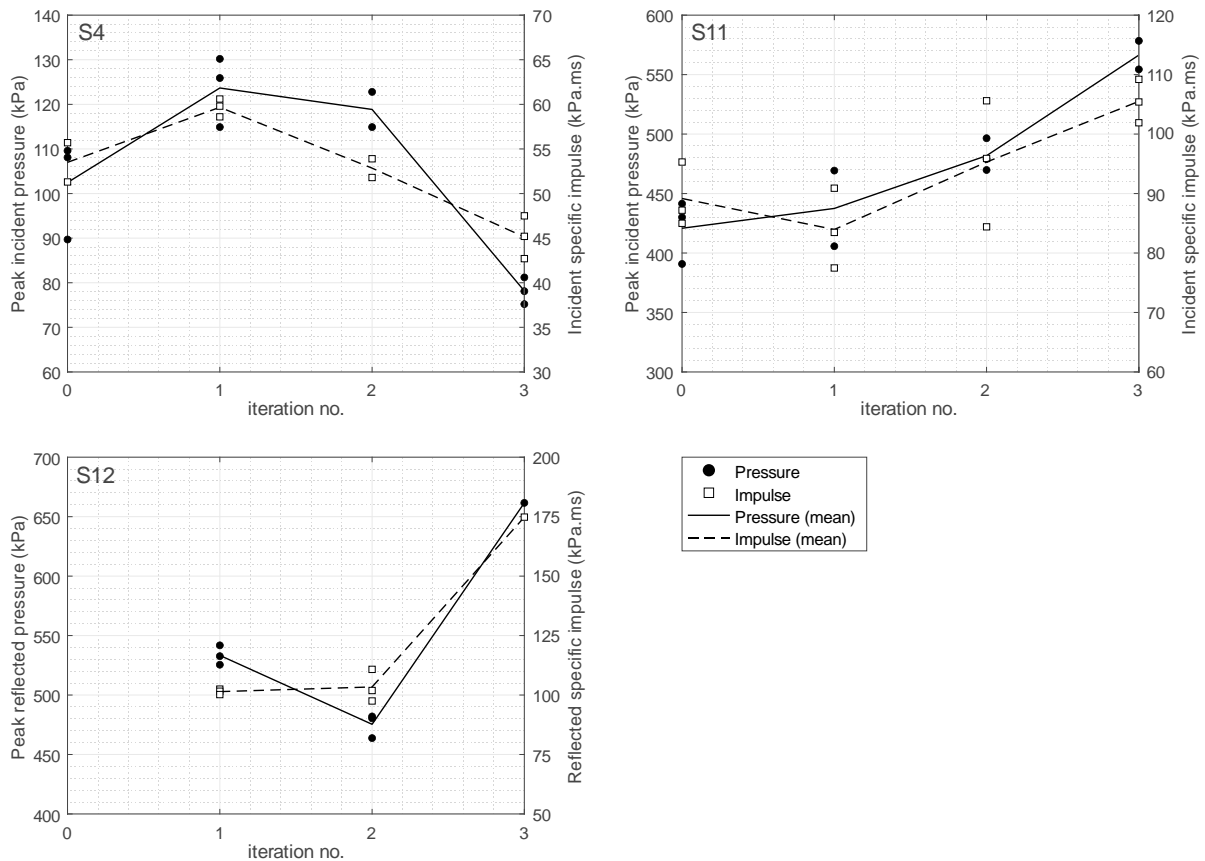
7

Figure 8. Compiled peak pressure and peak specific impulse [secondary y-axis] with increasing pre-fractal iteration for S4, S11, and S12 (250 g hemisphere at 1.25 m stand-off from the front-face of the central obstacle)

Summary and Conclusions

Blast events in urban settings presents a unique challenge to the protection engineering community: how to ensure blast effects are minimised without relying on obtrusive, hardened structures? One such solution is through the use of natural, sustainable protective solutions such as trees and hedges in place of, e.g., reinforced concrete blast walls.

Whilst there is emerging evidence that adequate blast mitigation can be achieved from such structures, the precise way in which the loading is mitigated has not yet been studied. This work has aimed to better understand the mitigation behaviour of natural sustainable blast walls through the rationalisation that such structures are self-similar, and therefore fractal-like.

A detailed experimental study was devised whereby the first three iterations of a Sierpinski carpet pre-fractal were subjected to blast loading from hemispherical PE4 charges and their blast attenuation behaviour studied. In particular, this article reports detailed results from three pressure sensors located either downstream, upstream, or on the face of the central obstacle.

It was found that whilst iterations 1 and 2 offered very little to no attenuation in terms of downstream pressure and impulse, iteration 3 exhibited considerable downstream mitigation; upwards of 20% reductions in pressure and impulse relative to the free-field values. This is attributed to a newly-observed mechanism termed 'trapping', where the blast is simultaneously forced along an elongated travel path, and reflects off and diffracts around numerous reflecting surfaces, ultimately reducing momentum in the original direction of travel and leading to downstream mitigation. This is fundamentally different to the mitigation mechanism of a simple, singular obstacle, which is predominantly through splitting of the wavefront and shielding effects. This proof-of-concept study demonstrates the possibility of using natural self-similar structures, such as trees and hedges, for sustainable and less intrusive blast protection in urban environments.

References

Alshammari OG et al. (2022), Mitigation of blast loading through blast–obstacle interaction, *International Journal of Protective Structures* [in press]

Bogosian D, Ferrito J and Shi Y (2002) Measuring uncertainty and conservatism in simplified blast models, In: *Proceedings of the 30th Explosives Safety Seminar*, Atlanta, GA, USA, 13-15 August

Farrimond DG et al. (2022), Time of arrival as a diagnostic for far-field high explosive blast waves, *International Journal of Protective Structures*, 13(2): 379-402

Gan EDJ, Remennikov A and Ritzel D (2021), Investigation of trees as natural protective barriers using simulated blast environment, *International Journal of Impact Engineering* 158: 104004

Gajewski T et al. (2022), Application verification of blast mitigation through the use of thuja hedges, *International Journal of Protective Structures*. 13(2): 363-378

Gebbeken N, Warnstedt P, and Rüdiger L (2018), Blast protection in urban areas using protective plants, *International Journal of Protective Structures*, 9(2): 226-247

Higham JE and Vaidheeswaran A (2022), Modification of modal characteristics in the wakes of blockages of square cylinders with multi-scale porosity, *Physics of Fluids*, 34: 025114

Isaac OS et al. (2022a), Experimental investigation of blast mitigation of pre-fractal obstacles, *International Journal of Protective Structures* [in press]

Isaac OS et al. (2022b), Blast wave interaction with structures – An overview, *International Journal of Protective Structures* [in press]

Larcher M and Casadeia F (2010) Explosions in complex geometries – A comparison of several approaches, *International Journal of Protective Structures*, 1(2): 169-196

Nguyen-Van V et al. (2021), Mechanical performance of fractal-like cementitious lightweight cellular structures: Numerical investigations, *Composite Structures*, 269: 114050

Rigby SE and Sielicki PW (2014), An investigation of TNT equivalence of hemispherical PE4 charges, *Engineering Transactions*, 62(4): 423-435

Rigby SE et al. (2014), A numerical investigation of blast loading and clearing on small targets, *International Journal of Protective Structures*, 5(3): 253-274

Rigby SE et al. (2020), Preliminary yield estimation of the 2020 Beirut explosion using video footage from social media, *Shock Waves*, 30: 671-675

Rose TA, Smith PD, and McLennan CP (2004), Blast loading and clearing on tall buildings, *Journal of Battlefield Technology* 7(3): 1-8

Smith PD (2010), Blast walls for structural protection against high explosive threats: A review, *International Journal of Protective Structures* 1(1): 67-84

Suzuki K et al. (2000), *Experimental studies on characteristics of shock propagation through a cylinder array*, The Institute of Space and Astronomical Science, Japan, Report No. 676

US Department of Defense (2008), *Structures to resist the effects of accidental explosions*, UFC 3-340-02, Washington DC, USA